Theory of spectroscopy in an optically pumped effusive vapor

T. M. Stace[1,*] and A. N. Luiten[2,†]
[1]*Department of Physics, University of Queensland, Brisbane, Queensland 4072, Australia*
[2]*Department of Physics, University of Western Australia, Perth, Western Australia 6009, Australia*
(Received 28 December 2009; published 29 March 2010)

We present a theoretical framework for studying spatially dependent absorption in a thermal vapor of multilevel atoms, of arbitrary optical thickness. The atomic state dynamics, governed by a standard atom-optical master equation, are self-consistently coupled to the axial evolution of the probe beam intensity and the effusive gas dynamics. We derive steady-state equations for the spatially varying distributions of atomic populations and the probe beam intensity. From the latter, absorption coefficients in both the saturated and unsaturated regimes can be calculated. We present solutions to the resulting equations at various levels of approximation, including an example of the full numerical solution of a saturated, optically thick vapor of three-level atoms, demonstrating a breakdown of Beer's law, among other measurable effects.

DOI: 10.1103/PhysRevA.81.033848 PACS number(s): 42.62.Fi, 32.70.Jz, 32.30.−r

I. INTRODUCTION

Atomic vapor cells are used widely across atomic, optical, and laser physics. For example, they find application in linear and nonlinear spectroscopy [1–4], laser frequency stabilization [5–7], primary thermometry [8,9], precision measurement [10,11], and more recently in quantum communication [12–14], quantum memories [15–17], and full quantum computation [18]. To predict and understand the key attributes that make the cells useful for such applications (e.g., the spectral lineshape of the absorption) the depth of the spectroscopic features, as well as decoherence related to atomic motion in quantum applications, it is essential to account for the role of gas dynamics and the interchange of energy between the optical and atomic systems.

Previous efforts have undertaken to do this under various restrictive assumptions. Some models assumed a uniform transverse beam intensity profile [2,19–21], or have not accounted for the intensity dependent absorption [22]. A common approach was the addition of a phenomenological relaxation rate between formally stable ground-state levels to account for beam transit effects (Ref. [23] and references therein). A number of numerically intensive models were also presented to solve the full density matrix model in the time domain [20,21,24]; however, those approaches have not taken into account the scattering of the light field by the atoms and the resulting evolution in intensity along the beam axis.

In contrast to previous work, in this article we develop a systematic theoretical framework that self-consistently couples multilevel atomic state dynamics, the optical beam intensity evolution, and the gas dynamics in the effusive regime[1]. Using this newly developed framework, we calculate the atomic population distributions and the optical intensity as a function of axial and radial coordinates for two- and three-level atoms. The results exemplify the essential physics of optical pumping in a saturated atomic vapor. Our approach applies to atomic vapors of arbitrary optical thickness, including regimes in which the atomic transitions are strongly saturated. Numerical solutions allow us to investigate high intensity beams entering optically thick vapor cells, where we observe the transition from saturated populations in which Beer's law fails, to weakly excited populations where Beer's law is re-established as the beam becomes strongly attenuated deep into the vapor. Importantly, the solutions to our coupled system of population dynamics and optical beam evolution show the effects of the gas dynamics to be very important in many of the applications listed previously. Ignoring them leads to qualitatively incorrect conclusions.

We begin by revisiting the standard derivation of the atomic population evolution equations for multilevel atomic populations in a time-dependent field, starting from the atom-optical master equation. Though our approach is applicable to any atomic model, to illustrate the essential physics of saturated atomic absorption we focus on a three-level system with two optically active states and a dark state. We couple the population dynamics to the thermal gas dynamics and the axial beam evolution, to derive coupled, nonlinear, integro-partial differential equations (PDE's) for the atomic populations and intensity profiles. From the axial variation of the intensity profile, we are able to directly compute various experimentally important quantities such as the absorption coefficient. We show that our approach gives standard results in the limits of weakly probed systems, for two-level atoms under uniform illumination, and for optically thin systems.

Finally, we describe a numerical method to solve for the spatially varying populations and laser intensity in a self-consistent way. To illustrate the method, we provide an example of a numerical calculation for the axial dependence of the pump intensity in a saturated vapor of three-level atoms. We solve for an initially Gaussian transverse beam profile, as well as a "top-hat" beam profile, and show significant quantitative differences in the saturated absorption of these two profiles. Importantly we show that our model predicts that the spatial variation of the optically pumped atomic populations will differ from that of the spatial dependence of the probing laser beam intensity. As atoms move through the beam, we see in our simulations a wake of excited atoms: The steady-state atomic populations are modified from their thermal equilibrium values

*stace@physics.uq.edu.au
†andre@physics.uwa.edu.au
[1]That is, where the mean-free path between atomic collisions is larger than the spatial extent of the vapor cell.

by the nearby laser beam, a phenomenon which seems to have been overlooked in other work [19,23,25].

II. ATOMIC MODEL

The dynamics of the state of a driven atomic system is governed by a generalization of the optical Bloch equations. We consider the problem of driving between two degenerate manifolds of hyperfine states, F_g and F_e. The master equation for the atomic density matrix ρ, takes the generic form

$$\frac{d\rho}{dt} = -i[H_{\text{atom}} + H_{\text{driving}}(t), \rho] + \sum_{j,k} \gamma_{j,k} \mathcal{D}[|g_j\rangle\langle e_k|]\rho, \tag{1}$$

where $\{|g_j\rangle\}$ and $\{|e_k\rangle\}$ are a basis of states for the hyperfine manifolds F_g and F_e, respectively, $\mathcal{D}[b]\rho = a\rho b^\dagger - (b^\dagger b\rho + \rho b^\dagger b)/2$ for any atomic operator b and $\gamma_{j,k}$ is the decay rate between states $|e_k\rangle$ and $|g_j\rangle$. In the absence of an external magnetic field,

$$H_{\text{atom}} = \frac{\omega_{jk}}{2}\left(\sum_k |e_k\rangle\langle e_k| - \sum_j |g_j\rangle\langle g_j|\right), \tag{2}$$

where ω_{jk} is the transition frequency. Finally,

$$H_{\text{driving}}(t) = \sum_{j,k} \vec{E}(t)\cdot\vec{\mu}_{jk}(|j\rangle\langle k| + |k\rangle\langle j|)/2, \tag{3}$$

where $\vec{E}(t)$ is the time-dependent driving field amplitude and $\vec{\mu}_{jk}$ is the dipole moment for the transition between $|e_k\rangle$ and $|g_j\rangle$. For future reference, we define the Rabi frequency $\Omega_{jk}(\vec{x}, t) = \vec{E}(t)\cdot\vec{\mu}_{jk}$.

Since the principal objective of this article is to elucidate the role of the effusive gas dynamics in saturation spectroscopy, we will simplify the generic atomic model above to a three-level system consisting of a ground-state manifold $\{|1\rangle, |2\rangle\}$ and a nondegenerate excited state $|3\rangle$. The transition $|1\rangle \leftrightarrow |3\rangle$ is driven coherently by an external laser. Level $|3\rangle$ suffers spontaneous emission to both $|1\rangle$ and $|2\rangle$. The dynamics of a driven three-level atom is then given by the standard quantum optical master equation[2]

$$\begin{aligned}\frac{d\rho}{dt} &= -i[H(t),\rho] + \gamma_{31}\mathcal{D}[|1\rangle\langle 3|]\rho + \gamma_{32}\mathcal{D}[|2\rangle\langle 3|]\rho,\\ H(t) &= \frac{\Delta}{2}(|3\rangle\langle 3| - |1\rangle\langle 1|) + \frac{\Omega(\vec{x},t)}{2}(|3\rangle\langle 1| + |1\rangle\langle 3|),\end{aligned} \tag{4}$$

where $\Delta = \omega_{13} - \omega_L$ is the detuning between the driven transition and the driving laser frequency and $\Omega \equiv \Omega_{13}$. In this model, we ignored direct transitions between levels $|1\rangle$ and $|2\rangle$, that is, $\gamma_{12} = 0$. This follows for atomic vapors such as Rb or Cs, in which states $|1\rangle$ and $|2\rangle$ are in the same hyperfine manifold, so transitions between them are dipole forbidden.

For our models, we assume that the diameter of the vapor cell is much larger than that of the pump beam. As a result, atoms approaching the beam are assumed to start in a thermal state

$$\rho(t = -\infty) \propto e^{-H_{\text{atom}}/k_B T}. \tag{5}$$

This is predicated on the known rapid rethermalization of atoms upon collision with the container walls [27–29]. Equation (5) represents the initial state of the atoms for our system.

The three-level atomic model described is sufficient to exemplify the essential physics of the problem of absorption of a saturating beam. We note that for the purposes of detailed, precise numerical simulations, it may well be necessary to include the full multilevel hyperfine structure in the atomic dynamics, at the cost of moderate additional computational overhead. Atomic models suitable for such simulations were described in detail in previous work [20,21,24] and Sec. 4.3 of Refs. [30] and [31].

A. Adiabatic Elimination

Equation (4) describes coherent dynamics associated with the driving as well as incoherent decay processes. In thermal systems, damping causes the off-diagonal elements of ρ to relax rapidly: They remain close to equilibrium with the populations at all times. These elements can thus be *adiabatically eliminated* by setting the time derivative to zero and solving the remaining (approximate) algebraic equation [32,33]. For clarity and to define notation, we recapitulate the derivation of the population rate equations by adiabatic elimination. For instance, the master equation gives

$$\dot{\rho}_{13}(t) = i\,\Delta\,\rho_{13} + i\,\Omega\,(\rho_{33} - \rho_{11}) - \Gamma\rho_{13}/2. \tag{6}$$

One approach to adiabatic elimination follows from setting $\dot{\rho}_{13} \to 0$, to yield an algebraic equation with solution

$$\rho_{13} = \frac{i\,\Omega}{i\Delta - \Gamma/2}(\rho_{33} - \rho_{11}). \tag{7}$$

This expression shows that the adiabatic elimination is self-consistent if $\Omega \ll \Delta$ or $\Omega \ll \Gamma$, so that the prefactor on the right-hand side (rhs) is small. Substituting these off-diagonal elements, which adiabatically follow the populations, into the ordinary differential equation (ODE's) for the diagonal population elements yields the well-known population rate equations

$$\frac{d\vec{P}}{dt} = M\cdot\vec{P}, \tag{8}$$

where $\vec{P} = \{P_1, P_2, P_3\} = \{\rho_{11}, \rho_{22}, \rho_{33}\}$ and

$$M = \begin{pmatrix} -\frac{\Omega^2/\Gamma}{1+4\Delta^2/\Gamma^2} & 0 & \beta\,\Gamma + \frac{\Omega^2/\Gamma}{1+4\Delta^2/\Gamma^2} \\ 0 & 0 & (1-\beta)\Gamma \\ \frac{\Omega^2/\Gamma}{1+4\Delta^2/\Gamma^2} & 0 & -\Gamma - \frac{\Omega^2/\Gamma}{1+4\Delta^2/\Gamma^2} \end{pmatrix},$$

where $\Gamma = \gamma_{13} + \gamma_{23}$ and $\beta = \gamma_{13}/\Gamma$ is the branching ratio to level 1. With respect our simple three-level system, if levels 1 and 2 are in the same hyperfine manifold (i.e., differ only in the m_F quantum number), then symmetry considerations require that $\gamma_{31} = \gamma_{32}$, so that $\beta = 1/2$. In atoms with degenerate hyperfine manifolds, β can be calculated from Sec. 4 of Refs. [30] or [34]. We shall employ Eq. (8) to

[2]See, e.g., Sec. 10.5 of Ref. [26].

calculate the atomic population dynamics, as is done in previous work [20,21,24], though we note in passing that with a modest increase in computational effort, we can solve the fully quantum dynamics in Eq. (4).

III. GAS DYNAMICS

Equations (4) and (8) apply to the atomic rest frame, in which a given atom sees a time-dependent field as it passes through the beam. In fact, we wish to consider a thermal ensemble of atoms characterized by a continuum of atomic velocity classes, denoted by the velocity vector $\vec{v}$. This thermal atomic gas is assumed to be at low pressure, so that the mean-free path between collisions is larger than the spatial extent of the vapor cell. This condition is easily met in commercial evacuated atomic vapor cells of, for example, Cs or Rb at room temperature. As a result, the vaporized atoms move ballistically and collision broadening is negligible.

To couple the atomic population dynamics to the gas dynamics, we transform from the atomic rest frame for atoms in velocity class $\vec{v}$ to the laboratory frame, in which the field is spatially varying, but static. The total time derivative in the atomic rest frame becomes the material derivative in the laboratory frame

$$d/dt \rightarrow \partial/\partial t + \vec{v} \cdot \vec{\nabla}. \tag{9}$$

At steady state in the laboratory frame, the partial time derivative vanishes, so that for each velocity class, we need to solve the PDE

$$\vec{v} \cdot \vec{\nabla}\, \vec{P}(\vec{x}; \vec{v}) = M \cdot \vec{P}(\vec{x}; \vec{v}). \tag{10}$$

Since the laser probes the average population at a point in space, we will ultimately average these populations over the velocity distribution.

The initial condition, Eq. (5), in the atomic rest frame, becomes a boundary condition in the laboratory frame. Atoms starting at position $\vec{x}_0$ well outside the beam have a population distribution $\vec{P}(\vec{x}_0, \vec{v}) = \vec{P}_{\text{therm}}$.

We note that, in what follows, we will use both transverse and cylindrical coordinate systems. In both systems, the z axis is coincident with the center of the laser beam. For a given velocity class $\vec{v}$, the transverse coordinate system is a rectilinear system with the τ axis parallel to the transverse velocity component (i.e., the velocity component orthogonal to the z axis). Velocities in the transverse coordinate system are defined by the two components v_z and v_τ, with $v_\tau^2 = v_x^2 + v_y^2$. The cylindrical coordinate system is the usual one, with the radial direction at each point defined to be both orthogonal to and passing through the z axis. The reason for the distinction is that the atomic motion in the effusive regime is rectilinear, while the intensity and average population distributions at each point in space are cylindrically symmetric. Thus the gas dynamics, Eq. (10), are most naturally solved in the transverse coordinate system, while the atomic population dynamics, Eq. (8), are most naturally solved in the cylindrical coordinate system. It should be noted that for a given atom, v_r and v_τ are different if its trajectory does not pass through the center of the beam: v_τ remains constant while v_r varies in time.

The principal effect of the transverse component of the velocity v_τ is to induce a time-dependent envelope in the atomic rest frame, as atoms in each velocity class traverse the beam profile. In the laboratory frame, this manifests as a wake of excited atoms which extend beyond the limits of the laser beam, in the direction of motion of the velocity class (see Fig. 4). The principal effect of the axial velocity is to induce a velocity-dependent Doppler shift, $\Delta \rightarrow \Delta_{v_z} = \Delta - v_z\omega/c$.

IV. AXIAL BEAM EVOLUTION

As light propagates through the medium, there are two important processes that occur. First, the light diffracts, according to the standard wave equation. Second, light is scattered from atoms in the vapor, so the total power transmitted decreases with optical depth. This latter effect leads to a nonlinear coupling between the optical beam intensity and the population dynamics: In regions of high intensity, the atomic populations saturate, so scattering is weak and so the beam is only weakly absorbed. Thus the optical scattering rate depends on the atomic populations, which depends on the local optical intensity, which depends in turn on the axial dependence of the scattering rate. We therefore need to self-consistently couple the axial beam evolution to the atomic population dynamics.

The electric field dynamics are given by the combined effect of these two processes

$$\frac{\partial E}{\partial z} = \left.\frac{\partial E}{\partial z}\right|_{\text{diff}} + \left.\frac{\partial E}{\partial z}\right|_{\text{abs}}. \tag{11}$$

As shown in the following, for the systems we are concerned with, absorption is the most significant of these two processes, and we may ignore the effects of diffraction.

A. Diffraction

An optical beam with a slowly varying envelope has an electric field of the form $E(\vec{x}, t) = \tilde{E}(\vec{x}, t)e^{i(\omega t - kz)}$. In the paraxial approximation, the envelope diffracts according to the Schrödinger-like, paraxial Helmholtz equation

$$\left.\frac{\partial \tilde{E}}{\partial z}\right|_{\text{diff}} = -\frac{i}{2k}\nabla_\tau^2 \tilde{E}, \tag{12}$$

where $\nabla_\tau^2 = \partial^2/\partial x^2 + \partial^2/\partial y^2$ is the transverse Laplacian [35].

The amount by which diffraction affects the beam profile is determined by the Fresnel number $N_F = a^2/(\lambda L)$, where a is the beam diameter, $\lambda = 2\pi/k$, and L is the length of the medium. If the Fresnel number is very large, then diffraction is negligible and the beam simply shadows the input profile.

This can be seen by estimating the amount by which the beam varies over an axial distance L, if the transverse profile varies from $\tilde{E}_0$ to 0 over a distance a. Then $|\nabla_\tau^2 \tilde{E}| \sim \tilde{E}_0/a^2$ and Eq. (12) gives

$$|\delta \tilde{E}| \sim L\left|\frac{\partial \tilde{E}}{\partial z}\right| \sim \frac{1}{4\pi N_F}\tilde{E}_0. \tag{13}$$

For an optical beam ($\lambda \sim 1\ \mu$m) of diameter 1 mm, passing through a 10-cm-long vapor cell, $4\pi N_F \sim 100$. Therefore, diffraction alone should change the beam profile by less than 1% over the length of the typical experiment.

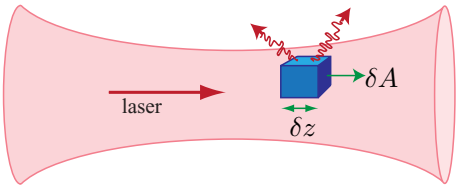

FIG. 1. (Color online) Light scattering off atoms within a small volume in the pump laser.

For the remainder of this article, we therefore ignore the effects of diffraction, making the approximation

$$\left.\frac{\partial E}{\partial z}\right|_{\text{diff}} \approx 0. \tag{14}$$

We note that the additional computational effort to include Eq. (12) in the simulations (described later) is small, so may be incorporated easily should it prove important for a particular situation.

B. Absorption

The optical pump beam is depleted as it propagates through the vapor. Consider a small volume $\delta V = \delta A\, \delta z$ of the gas, at position $\vec{x}$, as illustrated in Fig. 1. We assume that photons that are spontaneously emitted from the atoms are permanently scattered out of the beam. It follows that the number of photons scattered, δN, as the light propagates an axial distance $\delta z = c\,\delta t$ within the small volume is

$$\begin{aligned}\delta N(\vec{x}) &= \#(\text{stimulated } P_3 \to P_1) - \#(\text{absorbed } P_1 \to P_3)\\ &= [\bar{P}_3(\vec{x}) - \bar{P}_1(\vec{x})]\frac{\Omega^2(\vec{x})/\Gamma}{1+4\Delta^2/\Gamma^2}\rho_0\,\delta V\,\delta t,\end{aligned}$$

where ρ_0 is the atomic density and the over-bar denotes the velocity-averaged populations. The change in intensity of the beam is then

$$\begin{aligned}\delta I = \frac{\hbar\omega}{\delta A}\frac{\delta N}{\delta t} &= \hbar\omega(\bar{P}_3 - \bar{P}_1)\frac{\Omega^2/\Gamma}{1+4\Delta^2/\Gamma^2}\rho_0\,\delta z\\ \Rightarrow \frac{\partial I}{\partial z} &= \hbar\omega\rho_0(\bar{P}_3 - \bar{P}_1)\frac{\Omega^2/\Gamma}{1+4\Delta^2/\Gamma^2}.\end{aligned} \tag{15}$$

Ω^2 and I are proportional to one another, related by [36]

$$\frac{I}{I_{\text{sat}}} = \frac{2\Omega^2}{\Gamma^2}, \tag{16}$$

where $I_{\text{sat}} = c\epsilon_0\hbar^2\Gamma^2/(4|\mu|^2)$ (see, e.g., Sec. 4.2 of Ref. [30]), and is tabulated for several atomic transitions in Table I. Then

$$\frac{\partial(\Omega^2)}{\partial z} = \kappa(\bar{P}_3 - \bar{P}_1)\frac{\Omega^2}{(1+4\Delta^2/\Gamma^2)}, \tag{17}$$

where $\kappa = \hbar\omega\rho_0\Gamma/(2I_{\text{sat}})$. The rhs of this equation exhibits the nonlinear coupling between the optical beam intensity, proportional to Ω^2, and the atomic populations.

Including the velocity averaging in Eq. (17) explicitly yields

$$\frac{1}{\Omega^2}\frac{\partial(\Omega^2)}{\partial z} = \kappa\int d^3\vec{v}\, F_{v_0}(\vec{v})\frac{P_3(\vec{x};\vec{v}) - P_1(\vec{x};\vec{v})}{1+4\Delta_{v_z}^2/\Gamma^2}, \tag{18}$$

where $F_{v_0}(\vec{v}) = \pi^{-3/2}e^{-(v/v_0)^2}/v_0^3$ is the Maxwell-Boltzmann distribution with $v_0 = (2k_BT/m)^{1/2}$.

Since $\Omega \propto \tilde{E}$, we see that the electric field envelope decays according to

$$\left.\frac{1}{\tilde{E}}\frac{\partial\tilde{E}}{\partial z}\right|_{\text{abs}} = \frac{1}{2\,\Omega^2}\frac{\partial(\Omega^2)}{\partial z}. \tag{19}$$

Since the effects of diffraction are negligible, we will use Eq. (18) to completely specify the axial evolution of the beam.

V. NONDIMENSIONAL COUPLED DYNAMICS

The dynamical system of the atomic populations plus light satisfy the coupled integro-differential equations (8)[3] and (18). To begin setting up the problem for solution, we nondimensionalize space and time using $z^* = z/r_0$, where r_0 is some characteristic length (e.g., the radius of the Gaussian input beam), and $t^* = \Gamma t$ (and so, e.g., $\Omega^* = \Omega/\Gamma$). Then

$$\vec{v}^*\cdot\vec{\nabla}^*\,\vec{P} = M^*\cdot\vec{P}, \tag{20}$$

[3]Or Eq. (4) for the full quantum dynamics.

TABLE I. Typical values for the D_1 and D_2 transitions in ^{87}Rb and ^{133}Cs from data tabulated in Refs. [30,31]. Quantities below the line are temperature dependent and are evaluated at $T = 298$. The quantity $\pi\kappa K/2|_{\Delta=0} = \sqrt{\pi}\kappa/(2v)$ relates the dimensionless $\tilde{z}$ to dimensional z, and is the inverse absorption length in the unsaturated regime.

	^{87}Rb		^{133}Cs	
	D_1	D_2	D_1	D_2
ω ($2\pi\times$THz)	$2\pi\times 377$	$2\pi\times 384$	$2\pi\times 335$	$2\pi\times 352$
Γ (10^6 s^{-1})	36	38	28	33
I_{sat} (mW cm^{-2})	4.484	2.503	2.506	1.657
1-1 ρ_0 (m^{-3})	9.72×10^{15}		4.83×10^{15}	
κ (m^{-1})	155	299	95	178
v_0 (m s^{-1})	242		193	
Δ_{dop} ($2\pi\times$ MHz)	$2\pi\times 305$	$2\pi\times 311$	$2\pi\times 216$	$2\pi\times 227$
$v = \Delta_{\text{dop}}/\Gamma$	8.47	8.17	7.72	6.88
$\pi\kappa K/2\|_{\Delta=0}$ (m^{-1})	16.2	32.4	10.9	22.9

$$\frac{1}{\Omega^{*2}}\frac{d(\Omega^{*2})}{dz^*} = r_0\kappa \int d^3\vec{v}^*\, F_{v_0^*}(\vec{v}^*)\frac{P_3 - P_1}{\left(1+4\Delta_{v_z^*}^{*\,2}\right)}, \qquad (21)$$

where $v_0^* = v_0/(r_0\Gamma)$ and $\Delta_{v_z^*}^* = \Delta^* - v_z^* r_0\omega/c$. For a three-level atomic model

$$M^* = \begin{pmatrix} -\frac{\Omega^{*2}}{1+4\Delta^{*2}} & 0 & \beta + \frac{\Omega^{*2}}{1+4\Delta^{*2}} \\ 0 & 0 & (1-\beta) \\ \frac{\Omega^{*2}}{1+4\Delta^{*2}} & 0 & -1 - \frac{\Omega^{*2}}{1+4\Delta^{*2}} \end{pmatrix}.$$

For the remainder of this section the asterisks denoting nondimensional quantities will be dropped, and all variables will be assumed to be nondimensional.

In cylindrical coordinates,

$$\int d^3\vec{v} F_{v_0}(\vec{v}) = \int_0^{2\pi}\frac{d\theta}{2\pi}\int_{-\infty}^{\infty} dv_z F_{v_0}^{(z)}(v_z)\int_0^{\infty} dv_\tau F_{v_0}^{(\tau)}(v_\tau),$$

where

$$F_{v_0}^{(z)}(v_z) = \frac{e^{-(v_z/v_0)^2}}{\sqrt{\pi}v_0},$$
$$F_{v_0}^{(\tau)}(v_\tau) = \frac{2v_\tau e^{-(v_\tau/v_0)^2}}{v_0^2},$$

are the speed distributions for the axial v_z and transverse $v_\tau^2 = v_x^2 + v_y^2$ velocity components.

VI. WEAK BEAM AND VOIGT PROFILES

Far from saturation ($\Omega^{*2}(r,0) \ll 1$), P_1 is approximately constant everywhere, and $P_1 \gg P_3 \approx 0$. Then Eq. (21) becomes

$$\frac{\partial \ln\Omega^2}{\partial z} = r_0\kappa\int_{-\infty}^{\infty} dv_z \frac{F_{v_0^*}^{(z)}(v_z)}{1+4\Delta_{v_z}^2}[P_3(v_z) - P_1(v_z)] \qquad (22)$$

$$= -P_1\kappa c/\omega \int_{-\infty}^{\infty} d\Delta_{v_z}\frac{F_\nu^{(z)}(\Delta - \Delta_{v_z})}{1+4\Delta_{v_z}^2}$$

$$= -P_1\kappa\pi c\, V(\Delta,\nu)/2\omega. \qquad (23)$$

Here, the Voigt function V is a convolution of a Gaussian of (dimensionless) width $\nu = \Delta_{\rm dop}/\Gamma$ (where $\Delta_{\rm dop} = \omega v_0/c$), centered at Δ^*, with a Lorentzian of (dimensionless) width $1/2$ centered at the origin. This is the usual expression for unsaturated absorption. The solution is then given by a beam intensity that decays exponentially along the cell

$$\ln\Omega^{*2}(r,z) = -P_1\kappa\,\pi\,c\,V(\Delta,\nu)z/2\omega + \ln\Omega^{*2}(r,0).$$

This analysis shows that one should *only* expect the Voigt function to be a a good representation of the spectral absorption line when P_1 and P_3 are far from saturation. As described in detail in the Appendix, the first correction to Eq. (23) is $\cdots + \frac{d^2(P_3-P_1)}{d\Delta^2}\kappa\, c\,\mathcal{I}/(2\,\omega)$, where $\mathcal{I}$ is defined in Eq. (A1). We estimate the size of $P_3'' - P_1''$ from the steady-state solution for a two-level atom [see Eq. (31)], and find that for weak driving $P_3'' - P_1'' = -16\Omega^2 + O[\Omega^4]$. This correction to the Voigt lineshape takes the form of a doubly peaked function of Δ, shown in Fig. 7. The peak to trough height of the correction to the spectrum is $\sim\frac{\Omega^2\kappa c}{5\nu^3\omega}$. This should be compared to the height of the spectral line given by Eq. (23), which is $\sim\frac{\sqrt{\pi}\kappa c}{2\nu\omega}$. Taking the ratio of these, we find that the relative amplitude of the corrections is $\sim 0.2(\Omega^*/\nu)^2 = 0.2(\Omega/\Delta_{\rm dop})^2$.

VII. SATURATING MODELS

If the pump is strong enough that the populations are partially saturated, we need to include the effects of spatial variation in the populations. The equations become sufficiently complicated that we resort to numerical solutions. We make several controlled approximations and assumptions about the pump beam to simplify the numerical integration:

1. That the absorption length is much longer than the beam width, a. This means that the axial variation of the beam is small for a typical atom crossing the beam. This follows because the term $\partial\rho/\partial\tau$ in Eq. (20) varies much more over a length scale determined by a, which is much shorter than the term $\partial\rho/\partial z$, which varies over a distance of order the absorption length[4]. Then Eq. (20) becomes $v_\tau\partial\vec{P}/\partial\tau = M\cdot\vec{P}$.

2. That the Doppler broadening is much larger than the natural linewidth (i.e., $\nu \gg 1$). Making a change of variables from v_z to Δ_{v_z} in the velocity integrals gives

$$\int_{-\infty}^{\infty} dv_z F_{v_0^*}^{(z)}(v_z)\frac{P_3 - P_1}{1+4\Delta_{v_z}^2}$$
$$\approx \frac{c}{r_0\omega}F_{v_0^*}^{(z)}\left(\frac{c\Delta}{\Gamma r_0\omega}\right)\int_{-\infty}^{\infty} d\Delta_{v_z}\frac{P_3 - P_1}{1+4\Delta_{v_z}^2}$$
$$= 2K\int_0^{\infty} d\Delta_{v_z}\frac{P_3 - P_1}{1+4\Delta_{v_z}^2}, \qquad (24)$$

where we also used the symmetry of P_j with respect to Δ to halve the integration range and

$$K = \frac{c}{\omega r_0}F_{v_0^*}^{(z)}(c\Delta/\Gamma r_0\omega) = \frac{e^{-(\Delta/\Delta_{\rm dop})^2}}{\sqrt{\pi}\nu},$$

is a modified, nondimensional inverse-absorption length, which accounts for the reduced thermal population of atoms resonant with the laser around detuning Δ. Note that this approximation leads to spectra that have a strictly Gaussian tails at very large detuning, rather the the Lorentzian tails of the Voigt profile.

3. That the beam is initially cylindrically symmetric. Since the atomic velocity distribution is cylindrically symmetric, it follows that the velocity-averaged populations and the intensity will also be cylindrically symmetric. Then the angular integral appearing in the velocity averaging can be replaced by an angular integral over space,

$$\int_0^{2\pi}\frac{d\theta}{2\pi}P_j[\vec{x};\vec{v}(\theta)] = \int_0^{2\pi}\frac{d\theta}{2\pi}P_j(r\cos\theta, r\sin\theta, z; 0, v_\tau, v_z).$$

We therefore have the following set of coupled, nonlinear, integro-differential equations to solve

$$v_\tau\frac{\partial\vec{P}}{\partial\tau} = M\cdot\vec{P}, \qquad (25)$$

[4] A small fraction of atoms, $\sim a^2/4\pi(\text{abs. length})^2 \approx 0.1\%$ will have velocities that are nearly parallel to the beam, and so sample significant axial variation. This approximation ignores these.

$$\frac{\partial\,[\ln\Omega^2(r,z)]}{\partial z} = 2r_0\kappa\; K\; Q(r,z)$$

$$Q(r,z) = \int_0^{2\pi} d\theta \int_0^{\infty} d\Delta_{v_z} \int_0^{\infty} dv_\tau \frac{F_{v_0}^{(\tau)}(v_\tau)}{2\pi} \frac{P_3 - P_1}{1+4\Delta_{v_z}^2}, \tag{26}$$

where $P_j = P_j(r\cos(\theta), r\sin(\theta), z; 0, v_\tau, \Delta_{v_z})$, and recalling that M depends on Ω^2.

For the purpose of numerical integration, we make one further transformation, defining $\tilde{z} = (\pi\, r_0\kappa\, K/2)z^*$, so Eq. (26) becomes

$$\frac{\partial\,(\ln\Omega^2)}{\partial\tilde{z}} = (4/\pi)\,Q. \tag{27}$$

The quantity $\pi\kappa\, K/2$ is the inverse absorption length in the unsaturated regime, and is calculated in Table I for different atomic transitions. There are then only three quantities that we need to specify explicitly: β, v_0 and the initial beam profile, $\Omega_0^2(r)$. All other parameters in the problem (L, Γ, Δ, κ, etc.) are accounted for in the coefficient $r_0\kappa K$, and this simply determines the range of $\tilde{z}$ over which we need to integrate Eq. (26).

Absorption coefficient

The normalized absorbed power in a vapor of depth L is given by

$$\mathcal{A}_{\tilde{L}} = 1 - \frac{\int r\, dr\, \Omega^2(r,\tilde{L})}{\int r\, dr\, \Omega^2(r,0)}. \tag{28}$$

We use this to define the averaged absorption coefficient

$$\alpha = -\frac{\ln(1-\mathcal{A}_{\tilde{L}})}{\tilde{L}}. \tag{29}$$

For weak probe beams, Beer's law applies (i.e., $\mathcal{A}_{\tilde{L}} = 1 - e^{-\alpha\tilde{L}}$), and α will be independent of the optical depth of the vapor, $\tilde{L}$. For beams that partially saturate the transition, Beer's law fails, and α depends on $\tilde{L}$.

In a given numerical simulation (with a specified input beam profile and intensity) we are able to compute $\mathcal{A}_{\tilde{L}}$ and α for the range of $\tilde{L}$ over which we extend the numerical integration. By redimensionalizing $\tilde{L}$,

$$\tilde{L} = \frac{\sqrt{\pi}}{2}\frac{\kappa\, L}{\nu}\, e^{-(\Delta/\Delta_{\rm dop})^2}, \tag{30}$$

it follows that from the single simulation, we can also compute $\mathcal{A}$ and α as functions of the atom-laser detuning (via Δ), atomic density (via the κ dependence), temperature (via both κ and $\Delta_{\rm dop}$), or physical length (via L), as appropriate for the relevant experimental situation.

Because of saturation effects, if we wish to investigate the effect of varying the input probe beam power or intensity, we need to perform a different numerical simulation for each input beam setting.

VIII. SPECIFIC CASES

We now solve the system, subject to the approximations previously, in three different regimes. First, we solve the case of two-level atoms ($\beta = 1$) under uniform illumination. Then we solve for three-level atoms in optically thin and thick media taking into account the Gaussian beam profile.

A. Two-level atoms under uniform illumination

To get some intuition into the model, we simplify the system to the case of uniform illumination of infinite transverse extent. Then there is no r or τ dependence [i.e., $\rho = \rho(z;\Delta_{v_z})$, $\Omega^2 = \Omega^2(\tilde{z})$]. We also take $r_0 = \kappa^{-1}$. It follows that $\partial_\tau \vec{P} = 0$, so $M\cdot\vec{P} = 0$, and the atomic state is always at instantaneous equilibrium with the local field intensity. Note that in this regime there is no difference between the fully coherent dynamics and the incoherent dynamics derived by adiabatic elimination. In the three-level model discussed previously, in which level 2 is a dark state, the equilibrium atomic state is always $P_2 = 1$, $P_1 = P_3 = 0$. This corresponds to the condition in which all atoms reached state 2, and the vapor is transparent. The dynamics are then trivial.

On the other hand, for a two-level system (i.e., setting $\beta = 1$ to suppress decay to level 2), the equilibrium populations are

$$\begin{aligned} P_3(\tilde{z};\Delta_{v_z}) &= \frac{\Omega^2(\tilde{z})}{1+4\Delta_{v_z}^2+2\Omega^2(\tilde{z})} \\ \Rightarrow P_3 - P_1 &= -\frac{1+4\Delta_{v_z}^2}{1+4\Delta_{v_z}^2+2\Omega^2(\tilde{z})}. \end{aligned} \tag{31}$$

Then Eq. (27) becomes

$$\begin{aligned} \frac{d\,\Omega^2}{d\tilde{z}} &= -\frac{4}{\pi}\int_0^{\infty} d\Delta \frac{\Omega^2}{1+4\Delta^2+2\Omega^2} \\ &= -\frac{\Omega^2}{\sqrt{1+2\Omega^2}}. \end{aligned} \tag{32}$$

The solution to this ODE satisfies

$$\begin{aligned} \tilde{z}/2 = {} & \coth^{-1}\left(\sqrt{1+2\Omega^2(\tilde{z})}\right) - \sqrt{1+2\Omega^2(\tilde{z})} \\ & - \coth^{-1}\left(\sqrt{1+2\Omega_0^2}\right) + \sqrt{1+2\Omega_0^2}, \end{aligned}$$

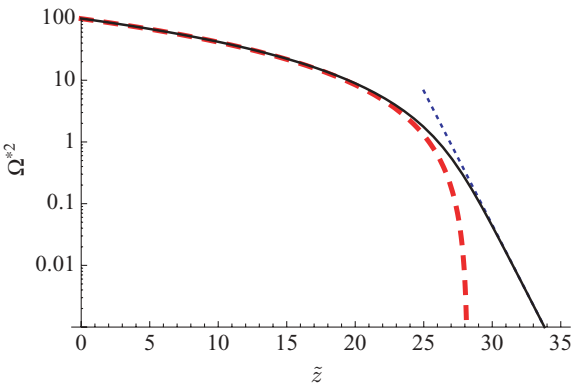

FIG. 2. (Color online) Solution and approximations to Eq. (32) showing the nondimensional Rabi frequency Ω^{*2} versus nondimensional length $\tilde{z} = (\pi\,\kappa\, K/2)z$ [also see Eq. (30)], for two-level atoms ($\beta = 1$) under uniform illumination. The dotted blue line is Beer's law, applicable to the unsaturated populations, and the red line is the highly saturated regime.

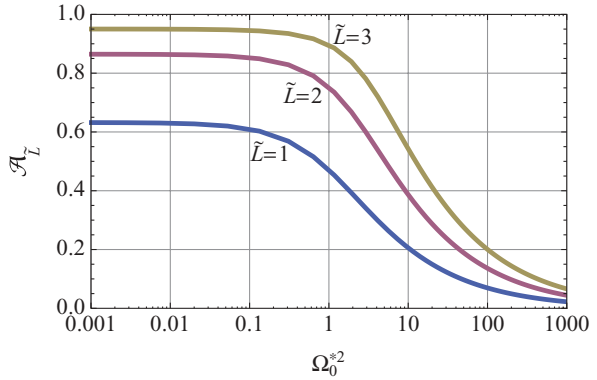

FIG. 3. (Color online) Fractional power absorption versus pump intensity, for different effective vapor lengths, $\tilde{L}$ for a two-level atom under uniform illumination. Both axes are nondimensional.

where $\Omega_0^2 = \Omega^2(0)$. The solution may be expressed in a simple form in the regimes for which $\Omega^2 \gg 1$ and $\Omega^2 \ll 1$

$$\Omega^2(\tilde{z}) \approx \begin{cases} \left(2\sqrt{1+2\Omega_0^2} - \tilde{z}\right)^2/8 & \text{if } \Omega^2 \gg 1, \\ \frac{2\sqrt{1+2\Omega_0^2}-2}{\sqrt{1+2\Omega_0^2}+1} e^{2(\sqrt{1+2\Omega_0^2}-1)} e^{-\tilde{z}} & \text{if } \Omega^2 \ll 1. \end{cases} \tag{33}$$

The boundary between these regions occurs around $\tilde{z}_b = 2\sqrt{1+2\Omega_0^2} - 2\coth^{-1}(\sqrt{1+2\Omega_0^2})$. The exact solution to Eq. (32) and these approximations [Eq. (33)] are shown in Fig. 2.

The fractional absorption is then

$$\mathcal{A}_{\tilde{L}} = \frac{\Omega_0^2 - \Omega^2(\tilde{L})}{\Omega_0^2}. \tag{34}$$

This is plotted in Fig. 3, showing both unsaturated ($\Omega_0^2 \ll 1$) and saturated ($\Omega_0^2 \gg 1$) regimes.

Using the approximate forms for Ω^2, valid in each of these regimes, we derive approximate expressions for the absorption coefficients

$$\mathcal{A}_{\tilde{L}} \approx \begin{cases} \frac{\left(2\sqrt{8\Omega_0^2}-\tilde{L}\right)\tilde{L}}{8\Omega_0^2} & \text{if } \Omega_0^2 \gg 1 \\ 1 - e^{-\tilde{L}} & \text{if } \Omega_0^2 \ll 1. \end{cases}$$

The former expression, for $\Omega_0^2 \gg 1$ represents the highly saturated regime. The latter, applicable to a weak probe, is simply Beer's law, with a dimensionless absorption coefficient of unity.

B. Optically thin three-level model

In the event that the vapor is optically thin, so that the fractional absorbed power is small, we use the approximation

$$\begin{aligned} \mathcal{A}_{\tilde{L}} &\approx -\tilde{L}\frac{\int r\,dr\,\partial_{\tilde{z}}\Omega^{*2}(r,0)}{\int r\,dr\,\Omega^{*2}(r,0)} \\ &= -\frac{4\tilde{L}}{\pi}\frac{\int r\,dr\,Q^*(r,0)\Omega^{*2}(r,0)}{\int r\,dr\,\Omega^{*2}(r,0)}, \end{aligned} \tag{35}$$

where the second step follows from Eq. (27). To evaluate the integral, we solve Eq. (25) numerically for the populations at $z = 0$, from which we derive Q. Redimensionalizing [using Eq. (30)] we find

$$\mathcal{A}_{\Delta} = -\frac{2}{\sqrt{\pi}}\frac{\kappa L}{v} e^{-(\Delta/\Delta_{\text{dop}})^2} \frac{\int r\,dr\,Q^*(r,0)\Omega^{*2}(r,0)}{\int r\,dr\,\Omega^{*2}(r,0)}. \tag{36}$$

The ratio of integrals in this expression is a numerical factor, and is straightforwardly computed numerically for specific values of the problem parameters. Clearly the absorption coefficient has a Gaussian dependence on the detuning, as expected in the regime $v \gg 1$.

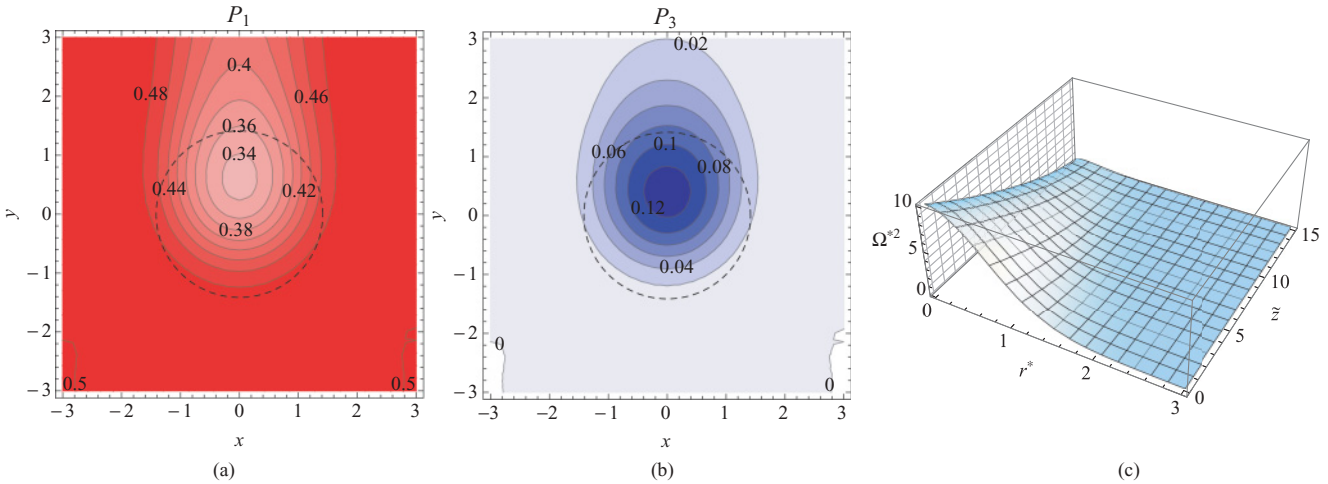

FIG. 4. (Color online) An example solution to the equations for a specific velocity class, $v_\tau = 1$ chosen to be parallel to the y axis, in an optically thick vapor with parameters $\beta = 0.8$, $\Omega_0^{*2} = 10$, and $v_0^* = 1$. The initial boundary condition is given by $\vec{P}(y = -3, x) = \vec{P}_{\text{therm}}$, where $y = -3$ is far outside the beam, (i.e., is effectively $-\infty$). Shown are contour plots of (a) P_1 and (b) P_3, evaluated at $\tilde{z} = 1$, $\Delta_{v_z}^* = 0$. The dotted circles at $r = \sqrt{2}$ represent the $1/e^2$ intensity of the input Gaussian beam profile. The intensity distribution $\Omega^2(r, z)$, in which all velocity classes are integrated over (c). Quantities shown are all dimensionless.

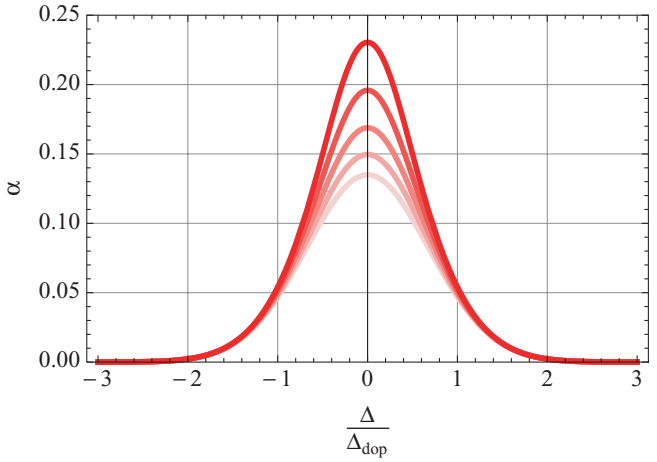

FIG. 5. (Color online) Absorption coefficient versus Δ for different axial positions in the vapor, that is, for $\tilde{L}|_{\Delta=0} = \sqrt{\pi}\kappa\, L/(2v)$ taking values 0 (lower curve) 3, 6, 9, 12, and 15 (upper curve), calculated from data in Fig. 4(c), using Eq. (29). The breakdown of Beer's law near zero detuning is evident: If it applied, these curves will fall on top of one another for all Δ. The lower curve, at $\tilde{L} = 0$, is a Gaussian: the absorption curves become increasingly less Gaussian.

C. Optically thick three-level model

For a vapor with finite absorption, we need to solve the full dynamical problem. Here, we take $r_0 = a$, the radius of the Gaussian input beam, so $\Omega_0^{*2}(r) = \Omega_0^{*2}\, e^{-r^2}$.

To numerically solve the nonlinear coupled equations (25) and (27), we adopt a self-consistent approach:

1. Guess $\Omega^{*2}(r, \tilde{z})$ [e.g., $\Omega^{*2}(r, \tilde{z}) = \Omega_0^{*2}\, e^{-r^2-\tilde{z}/2}$].

2. Solve Eq. (25) numerically, treating $\Omega^{*2}(r, \tilde{z})$ as a known function.

3. Calculate $Q(r, \tilde{z})$ found in step 2, by numerically integrating over the populations for all velocity classes and angles. In practice, Monte Carlo methods work well for this multidimensional integral.

4. Solve Eq. (27) numerically using Q determined in step 3, with initial condition $\Omega_0^{*2}(r) = \Omega_0^{*2}\, e^{-r^2}$.

5. Iterate back to step 2.

After several iterations, this process converges to self-consistent solutions for the populations and the intensity profile.

For numerical integration, the transverse boundaries should be chosen to be $\tau^* \gg 1$, so that the Gaussian beam profile is well represented. The axial integration should extend over $0 \leqslant \tilde{z}^* \leqslant \frac{\pi\Gamma c}{2\omega v_0}\kappa L = \pi\kappa L/2v$. The transverse velocity integration v_τ^*, should extend over a range several times v_0^* so that the Maxwellian velocity distribution is well represented. Finally, Δ_{v_z} should be integrated over $0 \leqslant \Delta_{v_z}^* \lesssim 10$, so that the Lorentzian is well represented.

To illustrate the simulation, we solve for a specific set of parameters[5]. Assuming $\Gamma \sim 10^6$/s, $v_0 \sim 10^3$ m/s at room temperature, we get $v_0^* \sim 1$ for a beam of radius $a = 1$ mm. We arbitrarily choose $\beta = 0.8$ and $\Omega_0^* = 10$. For numerical routines, in this example, we integrate over $-3 \leqslant x^*, y^* \leqslant 3$, $0 \leqslant \Delta_{v_z}^* \leqslant 10$, $0 \leqslant v_\tau^* \leqslant 3$, and $0 < \tilde{z} \leqslant 15$.

After a few iterations the self-consistent intensity profile converges to a relative variation between successive iterations of $\lesssim$0.1% at each spatial point, validating the procedure. Because we employ Monte Carlo integration routines, we do not expect more iterations to improve this figure further.

Example plots of the population and intensity distributions are shown in Fig. 4(a), 4(b), and 4(c). Since the medium is more absorptive at low intensities, there will be higher light absorption in the wings than at the center of the beam, leading to a transversal narrowing of the beam. This phenomenon is seen in the numerical simulations.

From $\Omega^2(r, z)$ in Fig. 4(c) one can directly calculate the absorption coefficient as a function of Δ, using Eq. (29). The result is shown in Fig. 5. The is the simulated result of an absorption spectrum obtained in an experiment in which the

[5]We employ the numerical PDE and integration routines provided in MATHEMATICA 7.0.

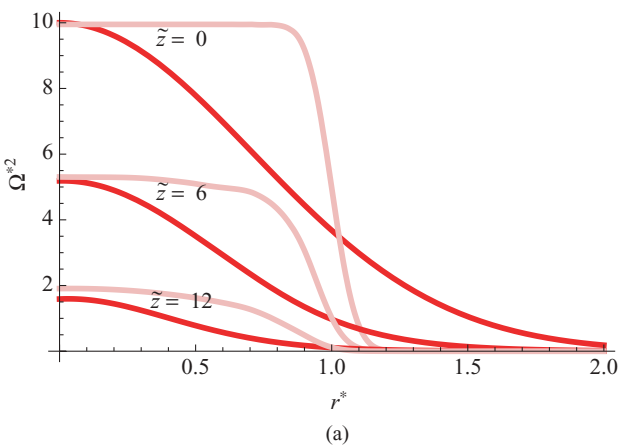

(a)

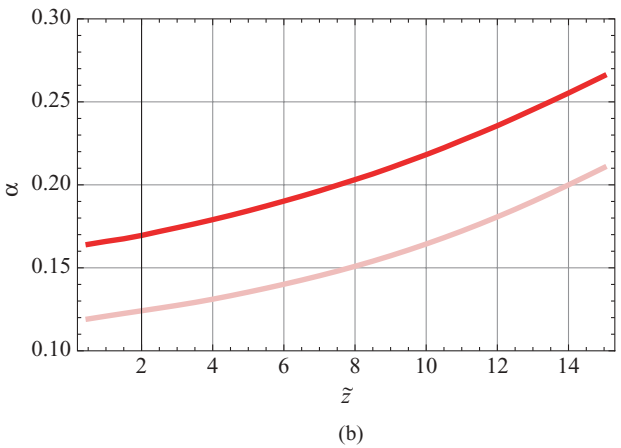

(b)

FIG. 6. (Color online) (a) Comparison of a Gaussian beam profile (dark curves) and an approximately "top-hat" beam profile (light curves), at different values of $\tilde{z}$, indicated, for $\Omega_0^{*2} = 10$, $\beta = 0.8$, and $v_0^* = 1$. (b) Absorption coefficient over distance, showing the quantitative difference in absorption between the Gaussian and top-hat profiles, for equal input powers.

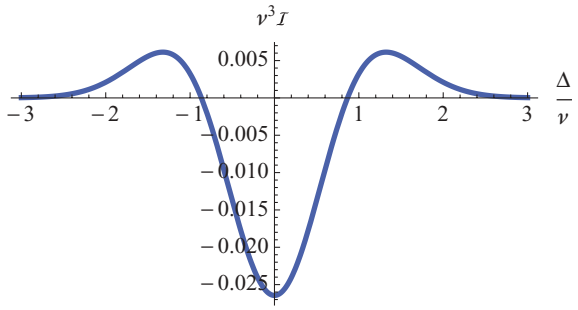

FIG. 7. (Color online) Generic form of the correction to the Voigt profile.

laser frequency is scanned through the transition, for different optical depths of the vapor (i.e., different vapor pressures, or different physical vapor cell lengths). Notably, the curves are not coincident around $\Delta = 0$, where the transition is saturated and Beer's law breaks down. In the wings, $\Delta > \Delta_{\text{dop}}$, the transition is not saturated, and the curves are coincident, indicating that Beer's law holds, in accordance with intuition. The lowest curve is a Gaussian, implying that the upper curves are more sharply peaked than a Gaussian distribution.

D. Comparison of top-hat and Gaussian profiles

Previous studies assumed a top-hat profile (constant over some finite range of r, then zero) for the transverse laser profile [2,19,20]. Our approach enables us to directly compare this assumption with the more realistic Gaussian profile. To make a fair comparison, we make the incident power of both profiles equal, so that

$$\Omega_0^{(G)^2}(r) = \Omega_0^{*2}\, e^{-r^2},$$
$$\Omega_0^{(U)^2}(r) = \Omega_0^{*2}\, H(1-r),$$

where H is a smooth approximation to the unit step.

Figure 6(a) shows the beam profile at different axial points, and Fig. 6(b) shows the absorption coefficient as a function of the axial distance. Clearly, the absorption is stronger for the Gaussian profile, which follows because a significant fraction of the beam power is in the wings of the profile, where the absorption is not saturated, and is therefore higher. As a consequence of the different axial dependence, we see that when combined with Eq. (30), the shape and amplitude of the absorption spectrum will be different in the two cases

IX. CONCLUSION

In this work we describe a model for saturation spectroscopy of an atomic vapor, including the effusive gas dynamics. The model reduces to known results in the appropriate limits, and provides a numerical approach to simulating nontrivial beam profiles. The axial and radial dependencies of the beam intensity is determined self-consistently with the population distribution, from which we directly compute absorption coefficients and spectra.

The main objective here is to develop a theoretical framework for self-consistently coupling the optical pump, atomic population, and gas dynamics. We therefore chose the simplest atomic model that demonstrates saturation phenomena, namely a vapor of three-level atoms. While this atomic model is overly simplistic for quantitative predictions in realistic atomic vapors, it nevertheless captures the important physics. Furthermore, the framework we developed easily adapts to more sophisticated atomic models, consisting of multiple degenerate hyperfine manifolds. We therefore anticipate that this work will serve as a useful theoretical and computational tool with which to understand high precision measurements of thermal atomic vapors.

ACKNOWLEDGMENTS

This work was funded by the Australian Research Council. We thank Eric May, Gar-Wing Truong, and Dustin Stewart for useful conversations.

APPENDIX: CORRECTIONS TO THE VOIGT PROFILE

If the excited state populations are nonnegligible, then there will be some dependence on the axial velocity, leading to corrections to the Voigt profile. These corrections can be derived from the observation that P_j is symmetric in Δ_{v_z}. Expanding P in powers of Δ_{v_z} yields the quadratic correction $P_j(\Delta_{v_z}) \approx P_j(0) + \Delta_{v_z}^2 P_j''(0)/2 + \cdots$. The correction to the rhs of Eq. (22) is then

$$\cdots + \frac{(P_3'' - P_1'')\kappa c}{2\omega} \int_{-\infty}^{\infty} d\Delta_{v_z}\, \Delta_{v_z}^2 \frac{F_\nu^{(z)}(\Delta - \Delta_{v_z})}{1 + 4\Delta_{v_z}^2}.$$

It is straightforward to show that

$$\begin{aligned}\mathcal{I} &\equiv \int_{-\infty}^{\infty} dx\, x^2 \frac{F_\nu^{(z)}(\Delta - x)}{1 + 4x^2} \\ &= \frac{\nu^4}{4}\frac{d^2V}{d\Delta^2} + \nu^2\Delta\frac{dV}{d\Delta} + \left(\Delta^2 + \frac{\nu^2}{2}\right)V.\end{aligned} \tag{A1}$$

To get some idea of the behavior of $\mathcal{I}$, we approximate the Voigt function as a Gaussian of variance $\nu^2 + 1/4$ [i.e., $V(\Delta, \nu) \approx e^{-\frac{\Delta^2}{\nu^2+1/4}}/\sqrt{\pi(\nu^2 + 1/4)}$], where the additional $1/4$ accounts for the Lorentzian contribution to the linewidth. Then

$$\mathcal{I} = \left(\frac{1}{8\sqrt{\pi}\,\nu} + \frac{4(\Delta/\nu)^2 - 3}{64\sqrt{\pi}\,\nu^3} + O[1/\nu^5]\right) e^{-\frac{\Delta^2}{\nu^2+1/4}}.$$

The first term simply represents a small rescaling of the amplitude of the Voigt profile (which we ignore), while the second term is a doubly peaked function, shown in Fig. 7. As illustrated, the peak to trough height of $\mathcal{I}$ is $\delta\mathcal{I} \approx 1/(40\,\nu^3)$.

[1] W. R. Bennett, Phys. Rev. **126**, 580 (1962).
[2] M. L. Harris, C. S. Adams, S. L. Cornish, I. C. McLeod, E. Tarleton, and I. G. Hughes, Phys. Rev. A **73**, 062509 (2006).
[3] D. Budker, D. F. Kimball, S. M. Rochester, and V. V. Yashchuk, Phys. Rev. Lett. **83**, 1767 (1999).
[4] W. Yang, D. B. Conkey, B. Wu, D. Yin, A. R. Hawkins, and H. Schmidt, Nat. Photon. **1**, 331 (2007).

[5] W. Y. Cheng, L. Chen, T. H. Yoon, J. L. Hall, and J. Ye, Opt. Lett. **27**, 571 (2002).
[6] M. Maric and A. Luiten, Opt. Lett. **30**, 1153 (2005).
[7] F. Benabid, F. Couny, J. C. Knight, T. A. Birks, and P. S. J. Russell, Nature (London) **434**, 488 (2005).
[8] C. Daussy, M. Guinet, A. Amy-Klein, K. Djerroud, Y. Hermier, S. Briaudeau, C. J. Bordé, and C. Chardonnet, Phys. Rev. Lett. **98**, 250801 (2007).
[9] G. Casa, A. Castrillo, G. Galzerano, R. Wehr, A. Merlone, D. DiSerafino, P. Laporta, and L. Gianfrani, Phys. Rev. Lett. **100**, 200801 (2008).
[10] S. Knappe, V. Gerginov, P. D. D. Schwindt, V. Shah, H. G. Robinson, L. Hollberg, and J. Kitching, Opt. Lett. **30**, 2351 (2005).
[11] W. C. Griffith, R. Jimenez-Martinez, V. Shah, S. Knappe, and J. Kitching, Appl. Phys. Lett. **94**, 023502 (2009).
[12] H. J. Briegel, W. Dur, J. I. Cirac, and P. Zoller, Phys. Rev. Lett. **81**, 5932 (1998).
[13] L.-M. Duan, M. D. Lukin, J. I. Cirac, and P. Zoller, Nature (London) **414**, 413 (2001).
[14] L.-M. Duan, Phys. Rev. Lett. **88**, 170402 (2002).
[15] D. F. Phillips, A. Fleischhauer, A. Mair, R. L. Walsworth, and M. D. Lukin, Phys. Rev. Lett. **86**, 783 (2001).
[16] I. Novikova, N. B. Phillips, and A. V. Gorshkov, Phys. Rev. A **78**, 021802(R) (2008).
[17] M. Hosseini, B. M. Sparkes, G. Hétet, J. Longdell, P. K. Lam, and B. C. Buchler, Nature (London) **461**, 241 (2009).
[18] S. D. Barrett, P. P. Rohde, and T. M. Stace, e-print arXiv:0804.0962.
[19] S. R. Shin and H.-R. Noh, J. Phys. Soc. Jpn. **78**, 084302 (2009).
[20] L. P. Maguire, R. M. W. van Bijnen, E. Mese, and R. E. Scholten, J. Phys. B **39**, 2709 (2006).
[21] B. T. H. Varcoe, R. T. Sang, W. R. Macgillivary, M. C. Stanage, and P. M. Farrell, J. Mod. Opt. **46**, 787 (1999).
[22] P. Siddons, C. S. Adams, C. Ge, and I. G. Hughes, J. Phys. B: At. Mol. Opt. Phys. **41**, 155004 (2008).
[23] J. Sagle, R. K. Namiotka, and J. Huennekens, J. Phys. B **29**, 2629 (1996).
[24] T. J. O'Kane, R. E. Scholten, P. M. Farrell, and M. R. Walkiewicz, Phys. Rev. A **59**, 4485 (1999).
[25] H. D. Do, G. Moon, and H.-R. Noh, Phys. Rev. A **77**, 032513 (2008).
[26] D. Walls and G. Milburn, *Quantum Optics* (Springer, New York, 2006).
[27] W. Franzen, Phys. Rev. **115**, 850 (1959).
[28] M. Shuker, O. Firstenberg, Y. Sagi, A. Ben-kish, N. Davidson, and A. Ron, Phys. Rev. A **78**, 063818 (2008).
[29] S. J. Seltzer, D. M. Rampulla, S. Rivillon-Amy, Y. J. Chabal, S. L. Bernasek, and M. V. Romalis, J. Appl. Phys. **104**, 103116 (2008).
[30] D. Steck, *Rubidium 87 d line data* (2003), http://steck.us/alkalidata/rubidium87numbers.1.6.pdf.
[31] D. Steck, *Cesium d line data* (2003), http://steck.us/alkalidata/cesiumnumbers.pdf.
[32] Y. Yamamoto and A. Imamoğlu, *Mesoscopic Quantum Optics* (Wiley Interscience, New York, 1999).
[33] A. S. Parkins and H. J. Kimble, J. Opt. B: Quantum Semiclass. Opt. **1**, 496 (1999).
[34] W. Happer, Rev. Mod. Phys. **44**, 169 (1972).
[35] B. Saleh and M. Teich, *Fundamentals of Photonics.* (Wiley, New York, 1991).
[36] B. E. Sherlock and I. G. Hughes, Am. J. Phys. **77**, 111 (2009).